

# Ab initio Molecular and Solid-state Studies of the Spin Crossover System [Fe(phen)<sub>2</sub>(NCS)<sub>2</sub>]

Samir F. Matar and Jean-François Létard

CNRS, Université de Bordeaux, ICMCB, 87 avenue du Docteur Albert Schweitzer, 33600 Pessac, France

Reprint requests to S. F. Matar. E-mail: s.matar@u-bordeaux1.fr

Z. Naturforsch. 2010, 65b, 565–570; received January 22, 2010

Ab initio computations are reported for both the isolated molecule and the extended solid within the density functional theory to assess the electronic structure and derived physical properties of [Fe(phen)<sub>2</sub>(NCS)<sub>2</sub>] in which Fe<sup>II</sup> is characterized by either one of two spin states, *i. e.* high spin (HS,  $t_{2g}^4 e_g^2$ ) and low spin (LS,  $t_{2g}^6 e_g^0$ ). For molecular HS and LS configurations, the characteristic IR and Raman spectra have been computed with vibrational frequencies magnitudes and their assignments in relative agreement with the experiment. For the extended solid, the equilibrium total energies reproduce the correct LS ground state. From the calculated equations of state for the two forms, a pressure-induced HS→LS transition is proposed.

**Key words:** Spin Crossover, DFT, Inorganic Complexes, Raman, IR, Equation of State

## Introduction

Few inorganic transition metal complexes exhibit two electronic states of their *d* electrons, the high spin state (HS) and the low spin state (LS). Switching between these two states is subjected to small energy magnitudes, and the transitions can be achieved with external constraints such as temperature and pressure as well as by applying light [1]. The observed behavior, referred to as spin crossover (SCO) and mainly studied in Fe<sup>II</sup> complexes [2, 3], has been widely investigated by research groups worldwide as well as in our Institute with several synthesized new materials [1, 4]. In this context, it is a current challenge to develop a model method useable to predict whether a given material is likely to exhibit a SCO phenomenon prior to its synthesis. Theoretical studies have already been related to the molecular approach [5–9], but to our knowledge there are no solid-state investigations of the electronic structure of the whole crystal system. The purpose of this work is to provide spectroscopic and electronic structure information from first principles on SCO systems for both the isolated molecule and the extended solid state. Such a complementary approach has been used in previous work on [Fe(btz)<sub>2</sub>(NCS)<sub>2</sub>] (btz: 2,2'-bis-4,5-dihydrothiazine) [10]. We focus here on the well characterized system [Fe(phen)<sub>2</sub>(NCS)<sub>2</sub>] where 'phen' stands for 1,10-phenanthroline, which

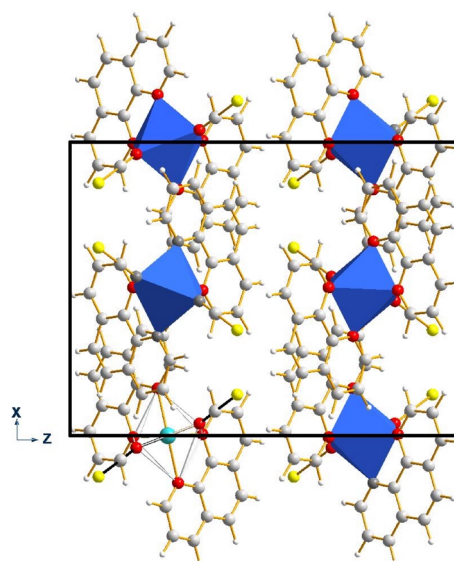


Fig. 1. Projection onto the crystallographic  $x0z$  plane of the orthorhombic [Fe(phen)<sub>2</sub>(NCS)<sub>2</sub>] structure (phen: 1,10-phenanthroline), with FeN<sub>6</sub> octahedra shown in blue. At bottom left, a molecular fragment used in molecular calculations is highlighted. Color scheme: Fe (blue-green), N (red), C (grey), S (yellow), H (white) (color online).

has a spin crossover temperature of  $T_{1/2} \approx 176$  K [11]. A projection of the orthorhombic crystal structure [11] is shown in Fig. 1, highlighting the octahedral environment of Fe and the molecular fragment used in the

calculations. The formula units (f. u.) on the edges are shared by two cells so that a total number of four f. u. per cell [11] is found.

### Theoretical Investigation of the Molecular System

Although the use of the Hartree-Fock (HF) approach has been shown to provide a good description of the molecular orbital and chemical bonding properties mainly in organic chemistry, it has been well established that the density functional theory (DFT) framework [12, 13] brings far more accurate results regarding the energetics and related properties. This is because the – compulsory – exchange and correlation (XC) effects are equally treated, albeit at a local level within the DFT, while only the exchange is well accounted for in HF although in a better way (exact exchange [14]) than in the DFT. Taking the best out of each of the two approaches led to improvements in *ab initio* calculations of molecules with the so called “hybrid functionals”. They consist of mixing exact HF exchange following Becke [14], and DFT-based correlation, following Lee, Yang and Parr with the so-called LYP correlation [15]. The B3LYP hybrid functional is among the most used. Its B3LYP\* modification by Reiher [7], in which the DFT local exchange is decreased, has been shown to bring similar accuracy of thermochemistry quantities as B3LYP.

After testing different functionals and basis sets through several molecular computations with the GAUSSIAN03 code [16], we found most accurate results for the energetics and the vibrational spectra in LS and HS states, respectively, with RB3LYP and UB3LYP (restricted for LS,  $S = 0$ , and unrestricted for HS,  $S = 2$ ) functionals and the 6-31g(d) basis set.

#### Optimization and energies

Firstly, the geometry of the molecule is optimized in both spin states and the results tested against the relative distances within the coordination sphere of the iron ions (Fig. 1). Although the final Fe–N distances do not translate a perfect octahedral  $O_h$ -like environment, we find on average that  $d_{LS} \langle \text{Fe–N} \rangle = 1.919 \text{ \AA}$  is smaller than  $d_{HS} \langle \text{Fe–N} \rangle = 1.983 \text{ \AA}$ . This is an expected result due to the volume increase of the divalent Fe coordination sphere arising from the occupation of anti-bonding  $e_g^*$  states with two unpaired electrons: LS ( $t_{2g}^6 e_g^0$ ) → HS ( $t_{2g}^4 e_g^2$ ). These average values agree with theoretical ones in the literature [17]

Table 1. [Fe(phen)<sub>2</sub>(NCS)<sub>2</sub>]: Calculated (calcd.) and experimental (exp.) Raman and infra-red frequencies ( $\text{cm}^{-1}$ ) with their assignments: a) low-spin state; b) high-spin state. Experimental values are from ref. [17].

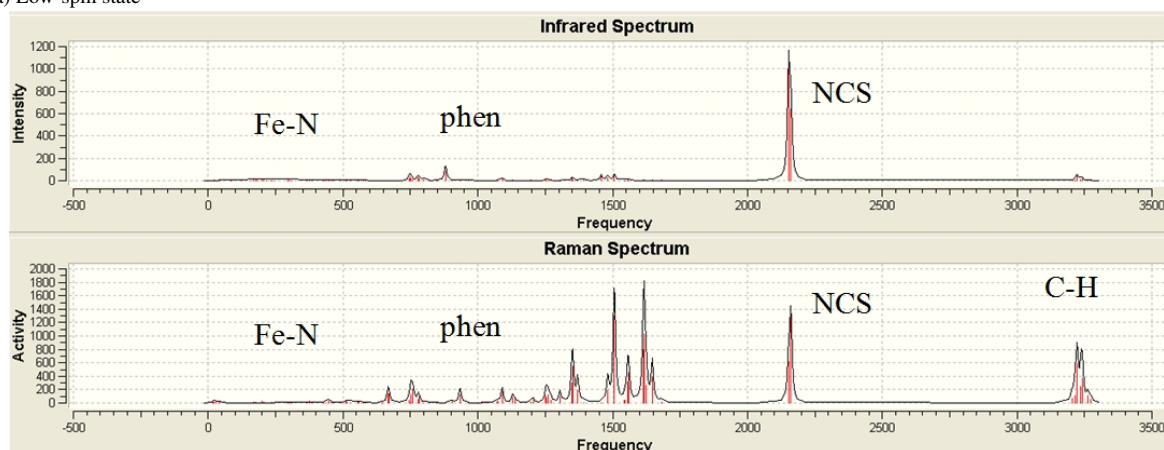
IR	IR	Raman	Raman	Assignment
calcd.	exp.	calcd.	exp.	
a) Low-spin state				
384	390	375	317	in-plane Fe–N elongation
754	726	760	725	out-of-plane phen cycle distortion
1506	1424	1506	1421	C–C elongation
2152	2107	2152	2107	antisymmetric NCS elongation
2161	2110	2161	2110	symmetric NCS elongation
b) High-spin state				
259	284	259	283	in-plane Fe–N elongation
753	725	735	725	out-of-plane phen cycle distortion
1463	1448	1470	1449	C–C elongation
2118	2062	2118	2062	antisymmetric NCS elongation
2126	2072	2126	2072	symmetric NCS elongation

where a so-called BP86 hybrid functional and triple- $\xi$  basis sets were used. Similarly, smaller computed values of the distances *versus* experiment were also found. The energy difference between LS and HS,  $\Delta E_{LS-HS} = 0.80 \text{ eV mol}^{-1}$ , favors the HS state. While the magnitude is within the range of the computed values by others [5, 6], its favoring of the high-spin state is a common error obtained with molecular calculations since the experimental ground state is the LS one [5, 6, 17]. Note that replacing Fe<sup>II</sup> by Zn<sup>II</sup> with no open  $d$  shell, giving a hypothetical [Zn(phen)<sub>2</sub>(NCS)<sub>2</sub>] complex, and optimizing the molecule with a similar basis set, results in an average  $d \langle \text{Zn–N} \rangle \sim 2.1 \text{ \AA}$ , which is larger than in both LS and HS Fe<sup>II</sup> complexes. This indicates the role of the crystal field for “ $d$ -active” ions such as divalent iron. The computed entropy change of  $\Delta S = 26.5 \text{ cal K}^{-1} \text{ mol}^{-1}$  is more than twice as large as the experimental value of  $\sim 12 \text{ cal K}^{-1} \text{ mol}^{-1}$  [18]. This drawback is also met in other computational approaches because in the calculations the individual fragment is examined without neighboring molecules.

#### Vibrational spectra

The optimized molecular setup is used to extract the vibrational properties. In Fig. 2 we show the calculated infrared (IR) and Raman spectra of the two spin states. The frequencies along the  $x$  axis are in units of wave numbers ( $\text{cm}^{-1}$ ). From left to right the spectral bands are assigned to in-plane elongation of Fe–N ( $\sim 300 \text{ cm}^{-1}$ ), out of plane distortion ( $\sim 700 \text{ cm}^{-1}$ ) and C–C elongation ( $\sim 1500 \text{ cm}^{-1}$ ) within the phen heterocycle. The most intense peaks around  $2100 \text{ cm}^{-1}$  for the symmetric and antisymmetric stretching elonga-

## a) Low-spin state



## b) High-spin state

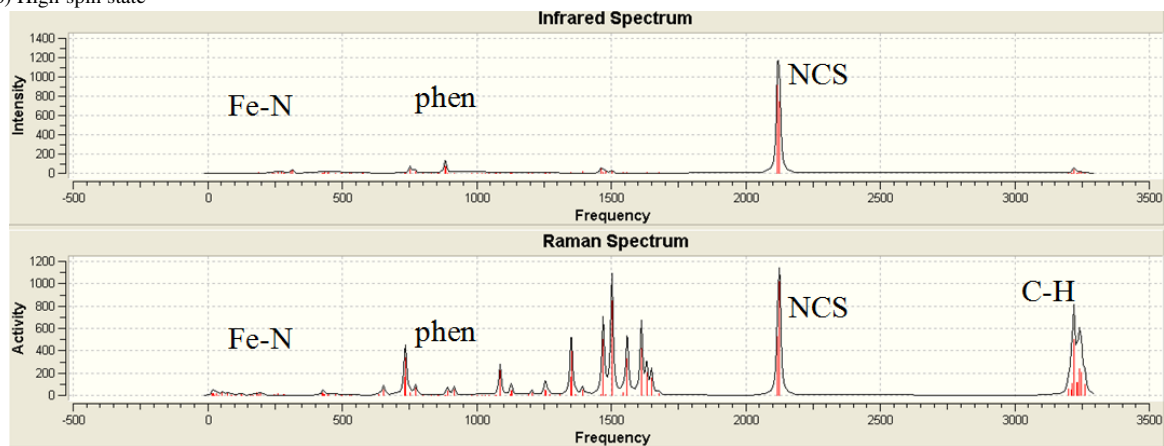


Fig. 2. Calculated infra-red and Raman spectra ( $\text{cm}^{-1}$ ) of  $[\text{Fe}(\text{phen})_2(\text{NCS})_2]$  in a) low-spin state and b) high-spin state.

tions characterize the  $\text{NCS}^-$  ligands when they are in *cis* configuration as it is the case for the presently studied complex. High intensity peaks around  $1500 \text{ cm}^{-1}$  for phen and other modes are mainly active in the Raman spectrum as for instance around  $3000 \text{ cm}^{-1}$  for C–H stretching modes in the phen heterocycle. The values are regrouped in Table 1 and confronted with experimental data from the literature. We note that the peak positions agree with only small deviations with experimental and theoretical data as given by Brehm *et al.* [17] for this complex. For instance, the anti-symmetric/symmetric  $\text{N}\equiv\text{C}$  stretching modes for the two  $\text{NCS}^-$  ligands of  $2162/2172 \text{ cm}^{-1}$ , are shifted by  $60 \text{ cm}^{-1}$  with respect to the experiment ( $2107/2110 \text{ cm}^{-1}$ ) but show the same trend of higher frequency for the symmetric stretching mode. This also stands for the HS spectra. However, they are systematically higher

for LS than for HS (Table 1), which can be considered as a designation of the spin state of the prepared complex. Consequently, the molecular calculations are found to provide correct spectroscopic identifications for the two spin states as far as the vibrations involve the internal behavior, while energies are less accurate when single, isolated molecular entities are considered.

### Solid-state Computations

Crystal structure studies of the low-temperature (LS) and high-temperature (HS) forms of  $[\text{Fe}(\text{phen})_2(\text{NCS})_2]$  were carried out by Gallois *et al.* [11]. They resulted in the orthorhombic space group *Pbcn* and  $Z = 4$  formula units (f. u.) per cell. At low temperature (130 K) the unit cell volume was  $2219 \text{ \AA}^3$  and at 293 K it was  $2338 \text{ \AA}^3$ .

Within DFT, the calculations of the electronic structures were carried out using the VASP package [19, 20]. The interactions between the ions and the electrons are described by using ultra-soft Vanderbilt pseudo-potentials (US-PP), and the effects of exchange and correlation XC were treated within local density approximation following the Ceperley and Alder scheme [21]. In the plane wave pseudo potential approach, the rapid variation of the potential near the nuclei is replaced by substituting the all-electron Hamiltonian with a smoother pseudo-Hamiltonian, which reproduces the valence energy spectrum. The PP allow a considerable reduction of the necessary number of plane waves per atom for transition metal and first row elements. Thus force and full stress tensor can be easily calculated and used to relax atoms into their ground state. The parallelized calculations, running on four processors, converged at an energy cut-off of 348 eV for the plane wave basis set in both forms. The  $k$ -point integration was carried out with a starting mesh of  $2 \times 2 \times 2$  up to  $4 \times 4 \times 4$  for convergence and relaxation to zero strains. This can be considered as high enough in view of the large number of atoms.

Besides total electronic energies and the density of states (DOS) we have obtained from the US-PP calculations a qualitative picture of the electron localization through a real space analysis of the electron distribution within the actual chemical system by comparing it with the free electron gas. This was done with the electron localization function (ELF) [22]. ELF is a normalized function which is close to 1 for strongly localized electrons (red spots),  $1/2$  for the free electron-like behavior (green spots), and close to 0 for no localization (blue zones).

#### Establishing the equations of state (EOS)

With experimental cell parameters and coordinates [11], a geometry relaxation was started for both forms. The results show little deviation with respect to the experiment for atomic coordinates. Focusing on the volumes, they show the same trends of lower volume for LS ( $V = 2145 \text{ \AA}^3$ ) versus HS forms ( $V = 2310 \text{ \AA}^3$ ). Smaller calculated values are expected from the use of PP's built within the LDA exchange correlation functional. In as far as it is based on the homogeneous electron gas, the LDA is *overbinding*, *i. e.* it tends to reduce interatomic spacing and energy gaps (*cf.* DOS section)

A better view of the behavior of both forms can be obtained from a set of energy versus volume ( $E, V$ )

calculations around experimental volumes. This is because the calculated total energy pertains to the cohesive energy within the crystal since the solution of the Kohn-Sham DFT equations yield the energy with respect to infinitely separated electrons and nuclei. In as far as the zero of energy depends on the choice of the pseudo-potentials, somehow it becomes arbitrary; *i. e.* it is shifted, not scaled. But the energy derivatives remain unaltered as well as the equations of state (EOS). For this reason, one needs to establish the EOS and extract the fit parameters for an assessment and confrontation of the equilibrium values. This justifies the protocol followed in the process of the calculations, *i. e.* a geometry relaxation followed by an establishment of the respective EOS's.

The resulting  $E = f(V)$  curves show a quadratic variation which can be fitted with Birch equation of state (EOS) to the 3<sup>rd</sup> order [23]:

$$E(V) = E_0(V_0) + [9/8]V_0B_0\left[\left(\frac{V_0}{V}\right)^{2/3} - 1\right]^2 + [9/16]B_0(B' - 4)V_0\left[\left(\frac{V_0}{V}\right)^{2/3} - 1\right]^3$$

where  $E_0$ ,  $V_0$ ,  $B_0$  and  $B'$  are the fit values: the equilibrium energy, the volume, the zero-pressure bulk modulus and its pressure derivative, respectively. The results are shown in Fig. 3 for the curves and the fit results. The LT curve lies at lower energy and smaller volume than HS pointing to LS as the actual ground state. Examining the values in the insert, the energy difference favors the LS state by  $-2.86 \text{ eV}$  per 4 f. u., *i. e.*,  $-0.71 \text{ eV}$  per f. u. This is interesting in view of the  $\Delta E = 0.80 \text{ eV}$  per f. u. found from molecular calculations albeit with opposite sign. The difference in absolute magnitude may have technical, method-inherent,

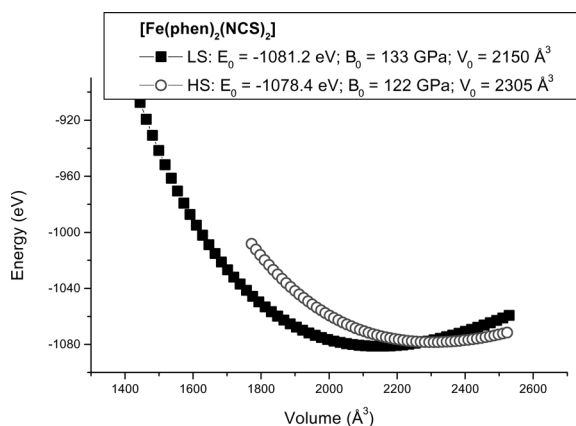


Fig. 3. Energy versus volume results for the LS and HS forms with Birch 3<sup>rd</sup> order EOS fit results.

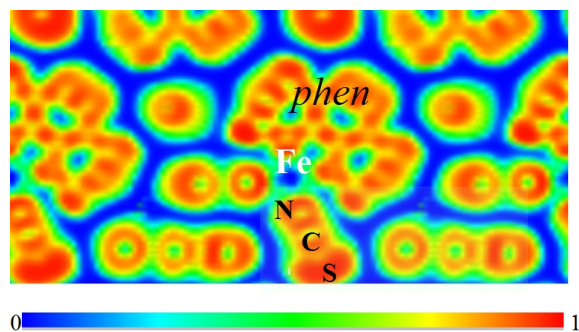


Fig. 4. Electron localization function (ELF slice) plot of [Fe(phen)<sub>2</sub>(NCS)<sub>2</sub>]. See Fig. 1 for retracing the molecule, and the text for color labeling (color online).

as well as fundamental origins. For the former, the use of different functionals belonging to each kind of method (hybrid B3LYP *versus* DFT-native LDA) can be the origin of the difference. For the latter, lattice effects not accounted for in molecular calculations can be invoked. In this context it is interesting to see how the electrons are localized within the unit cell containing four f. u. This can be visualized from the ELF contours given in Fig. 4 which can be seen to closely retrace the molecular entity of the complex in Fig. 1, with strong localization toward the phen and NCS<sup>-</sup> ligands. A marked feature is the presence of zero localization blue zones around the molecular entities, which suggests that they are isolated from each other. Although not seen here, this does not exclude hydrogen bonding involving for instance negatively charged terminal S in NCS as it can be seen from the large red spots.

Pressure derivatives of the bulk modulus values  $B'$  are close to 4 in both forms. The bulk modulus is larger for the LS form in agreement with its lower volume. The range of magnitudes of 120–130 GPa is not large compared to layered bi-dimensional systems [24] but the computed  $B_0$  values are larger than in alloy systems [25]. The equilibrium energy/volume results allow evaluating a transition pressure HS→LS which amounts to  $\sim 28$  kbar. This value is within the range generally observed, between 10 and 50 kbar [26]. Lastly we point out that the calculations are zero entropy so that they do not allow a direct access to transition temperatures.

#### Density of states (DOS)

At another level of solid-state calculations of the crystal structure, the electronic density of states (DOS) can be obtained as an illustration of the “organized

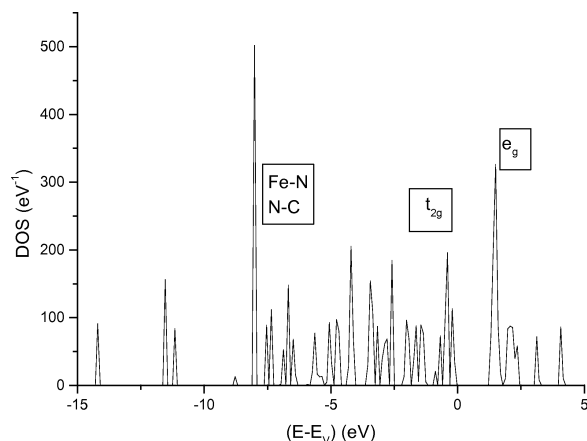


Fig. 5. Total DOS for orthorhombic [Fe(phen)<sub>2</sub>(NCS)<sub>2</sub>] in its low-spin ground state.

solid”. The total DOS are shown for the LS ground state configuration in Fig. 5. The major feature is the low dispersion of the DOS peaks which is descriptive of a molecular system, *i. e.* in opposition to a metal or an intermetallic system [25], where the DOS are broadened. Along the  $x$  axis the energy is counted with respect to the top of the valence band,  $E_V$  – not equivalent to the Fermi level  $E_F$  which characterizes a metallic system –, since the system is found to be an insulator with a gap of  $\sim 1.5$  eV in both spin states. This was also observed for [Fe(btz)<sub>2</sub>(NCS)<sub>2</sub>] [10], calculated with a smaller gap using the all-electrons ASW (augmented spherical wave) method [27]. This energy value is not to be considered quantitatively because the LDA XC functional tends to underestimate gaps. The  $O_h$ -like crystal field features for Fe<sup>II</sup> are exhibited in the DOS: the top of the valence band (VB) and the bottom of the conduction band (CB) are involved with Fe  $d$  states on both sides of the energy gap with empty  $e_g$ -like manifolds within the CB and occupied  $t_{2g}$ -like states at the top of the VB. The lower part of the VB is involved in Fe–N and N–C bonding. At lower energies, the  $s$ -like states of non-metals are found.

#### Concluding Remarks

The presented original double approach involving molecular and all solid-state calculations has been shown to bring complementary information on a complex inorganic system which undergoes a spin state transition HS→LS. From computations carried out for the isolated molecule, the IR and Raman spectra have been computed with trends of magnitudes and assign-

ments similar to those found in experiments. Such theoretical spectra can be helpful to experimentalists, for instance in micro-Raman spectroscopy. However, an HS ground state is obtained from energy differences and not the actual LS probably because contacts between molecules such as hydrogen bonds and other cooperative phenomena need to be considered. Heavier computations with massively parallel processing (MPP), involving two adjacent or more molecules may allow an improvement of the results; these are underway.

By contrast, computing the whole crystal system with four adjacent formula units leads to a correct LS

ground state, thus pointing out the importance of accounting for the system in a crystal array. It is characterized by an insulating behavior from the analysis of the density of states. From the equilibrium fit values of the respective equations of states, a pressure-induced HS→LS transition can be proposed.

#### Acknowledgements

Critical discussions with Prof. Ph. Guionneau are acknowledged. Computations were carried out on the mainframe computers of the University Bordeaux 1 MCIA (former M3PEC) facilities.

- 
- [1] Ch. Baldé, C. Desplanches, A. Wattiaux, Ph. Guionneau, Ph. Gütllich, J.-F. Létard, *Dalton Trans.* **2008**, 20, 2702.
- [2] A. Bousseksou, J.J. McGarvey, F. Varret, J.A. Real, J.-P. Tuchagues, A.C. Dennis, M.L. Boillot, *Chem. Phys. Lett.* **2000**, 318, 409.
- [3] For a general review, see: Ph. Gütllich, H.A. Goodwin (Eds.), *Spin Crossover in Transition Metal Compounds, Topics in Current Chemistry*, Vol. 233, Springer, Berlin, Heidelberg, New York, **2004**.
- [4] J.-F. Létard, P. Guionneau, L. Rabardel, J.A.K. Howard, A.E. Goeta, D. Chasseau, O. Kahn, *Inorg. Chem.* **1998**, 37, 4432.
- [5] V.K. Pálfi, Th. Guillon, H. Paulsen, G. Molnar, A. Bousseksou, *C.R. Chimie* **2005**, 8, 1317.
- [6] H. Paulsen, L. Duelund, H. Winkler, H. Toftlund, A.X. Trautwein, *Inorg. Chem.* **2001**, 40, 2201.
- [7] M. Reiher, *J. Chem. Phys.* **2002**, 117, 4729.
- [8] M. Reiher, *Inorg. Chem.* **2002**, 41, 6928
- [9] H. Paulsen, R. Benda, C. Herta, V. Schünemann, A.I. Chumakov, L. Duelund, H. Winkler, H. Toftlund, A.X. Trautwein, *Phys. Rev. Lett.* **2001**, 86, 1351.
- [10] L. Kaban, S.F. Matar, M. Zakhour, J.F. Létard, *Z. Naturforsch.* **2008**, 63b, 154.
- [11] B. Gallois, J.A. Real, C. Hauw, J. Zarembowitch, *Inorg. Chem.* **1990**, 29, 1152.
- [12] P. Honenberg, W. Kohn, *Phys. Rev. B* **1964**, 136, 864.
- [13] W. Kohn, L.J. Sham, *Phys. Rev. A* **1965**, 140, 1133.
- [14] A.D. Becke, *J. Chem. Phys.* **1988**, 88, 2547.
- [15] C. Lee, W. Yang, R.G. Parr, *Phys. Rev. B* **1988**, 37, 785.
- [16] M.J. Frisch, G.W. Trucks, H.B. Schlegel, G.E. Scuseria, M.A. Robb, J.R. Cheeseman, J.A. Montgomery, Jr., T. Vreven, K.N. Kudin, J.C. Burant, J.M. Millam, S.S. Iyengar, J. Tomasi, V. Barone, B. Mennucci, M. Cossi, G. Scalmani, N. Rega, G.A. Petersson, H. Nakatsuji, M. Hada, M. Ehara, K. Toyota, R. Fukuda, J. Hasegawa, M. Ishida, T. Nakajima, Y. Honda, O. Kitao, H. Nakai, M. Klene, X. Li, J.E. Knox, H.P. Hratchian, J.B. Cross, V. Bakken, C. Adamo, J. Jaramillo, R. Gomperts, R.E. Stratmann, O. Yazyev, A.J. Austin, R. Cammi, C. Pomelli, J.W. Ochterski, P.Y. Ayala, K. Morokuma, G.A. Voth, P. Salvador, J.J. Dannenberg, V.G. Zakrzewski, S. Dapprich, A.D. Daniels, M.C. Strain, O. Farkas, D.K. Malick, A.D. Rabuck, K. Raghavachari, J.B. Foresman, J.V. Ortiz, Q. Cui, A.G. Baboul, S. Clifford, J. Cioslowski, B.B. Stefanov, G. Liu, A. Liashenko, P. Piskorz, I. Komaromi, R.L. Martin, D.J. Fox, T. Keith, M.A. Al-Laham, C.Y. Peng, A. Nanayakkara, M. Challacombe, P.M.W. Gill, B. Johnson, W. Chen, M.W. Wong, C. Gonzalez, J.A. Pople, GAUSSIAN03 (revision C.02), Gaussian Inc., Wallingford, CT (USA) **2004**.
- [17] C. Brehm, M. Reiher, S. Schneider, *J. Phys. Chem. A* **2002**, 106, 12024.
- [18] M. Sorai, S. Seki, *J. Phys. Chem. Solids* **1975**, 35, 555.
- [19] G. Kresse, J. Hafner, *Phys. Rev. B* **1993**, 47, 558.
- [20] G. Kresse, J. Furthmüller, *Phys. Rev. B* **1996**, 54, 11169.
- [21] D.M. Ceperley, B.J. Alder, *Phys. Rev. Lett.* **1980**, 45, 1196.
- [22] A.D. Becke, K.E. Edgecombe, *J. Chem. Phys.* **1990**, 92, 5397.
- [23] F. Birch, *J. Geophys. Res.* **1978**, 83, 1257.
- [24] M. Mattesini, S.F. Matar, *Phys. Rev. B* **2002**, 65, 075110.
- [25] S.F. Matar, *Solid State Sci.* **2010**, 12, 59.
- [26] Ph. Guionneau, unpublished results, **2010**; private communication.
- [27] V. Eyert, *The Augmented Spherical Wave Method – A Comprehensive Treatment, Lect. Notes Phys.*, Vol. 719, Springer, Berlin Heidelberg, **2007**.